Science of the Total Environment 999 (2025) 180348

Contents lists available at ScienceDirect

Science of the Total Environment

journal homepage: www.elsevier.com/locate/scitotenv

Impacts of El Niño on the sediment balance of a transgressive dune-beach system

Amaia Ruiz de Alegría-Arzaburu [a,*], Susana Costas [b], Irene Delgado-Fernández [c]

[a] Universidad Autónoma de Baja California, Instituto de Investigaciones Oceanológicas, Ensenada, Baja California 22860, Mexico
[b] Universidade do Algarve, Centre for Marine and Environmental Research (CIMA), Aquatic Research Network (ARNET), Campus de Gambelas, Edifício 7, Faro, Portugal
[c] Universidad de Cádiz, Facultad de Ciencias del Mar y Ambientales, Puerto Real, Cádiz 11510, Spain

HIGHLIGHTS

- El Niño events caused episodic landward shifts of the coastline.
- The dune ridge migrated landward 5 m/yr, decoupling from the beach.
- Sediment moved landward from the berm to the dune, maintaining a positive sand budget.
- Shoreface inputs supported long-term balance of the transgressive system.

GRAPHICAL ABSTRACT

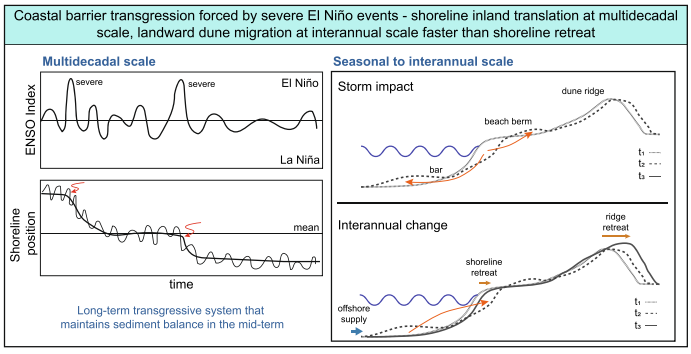

ARTICLE INFO

Keywords:
Morphodynamics
Sediment transport
Storms
Shoreline evolution
Shoreface
Beachface

ABSTRACT

Understanding long-term evolution of sandy coasts requires in-depth analysis of the sediment balance from the shoreface to the beach and dune. While storms typically erode the subaerial beach, they can also contribute sediment from deeper waters to the coastal budget. Here, we explore the impacts of El Niño-driven storms on the sediment balance across the entire shore-beach-dune profile. Satellite-derived shorelines (1984–2020) were combined with sixty-six topo-bathymetric surveys (2014–2020), along a 1 km stretch of southern Ensenada beach (Baja California). Forcing conditions were characterized using hourly wave and wind data. Multi-decadal shoreline data reveal that high-energy El Niño events have led to punctuated landward coastline translation. Interannual topo-bathymetric surveys show an active 8 to 9.5 m-high dune ridge along the upper part of the profile, migrating landward at a rate of 5 m/yr. This migration gradually decoupled the dune from the beach, occasionally creating space across the dune toe area for the formation of incipient dunes that eventually merged with the main ridge. The sediment budget analysis indicates a one-way landward transfer of sediment from the winter-berm to the dune. Interestingly, the overall shore-beach-dune sand budget remained positively balanced, with an increase of ≈40 m^3/m related to sediment availability from deeper waters and onshore transport from the lower shoreface. Shoreline trends and sediment budgets illustrate a long-term transgressive system capable of

* Corresponding author.
E-mail address: amaia@uabc.edu.mx (A. Ruiz de Alegría-Arzaburu).

https://doi.org/10.1016/j.scitotenv.2025.180348
Received 15 May 2025; Received in revised form 4 August 2025; Accepted 22 August 2025
Available online 28 August 2025

maintaining sedimentary balance in the mid-term. Increased storm activity and sea-level rise are expected to accelerate beach-dune transgression, which could retain sediment balance if offshore inputs persist.

1. Introduction

Understanding sediment exchanges and budgets across the shore-beach-dune profile at different temporal scales is key to identifying potential evolutionary trajectories that coastal barriers may adopt as they adapt to external forces such as sea-level rise and storm impacts. It is generally accepted that the emerged part of the beach erodes in response to storms, with erosion sometimes reaching the dune, and that the eroded sand is transported offshore forming submerged bars (Vidal-Ruiz and Ruiz de Alegría-Arzaburu, 2020). These bars may eventually return to the emerged beach under favorable wave conditions (Ruiz de Alegría-Arzaburu and Vidal-Ruiz, 2018). However, in contrast to this generally accepted model, storms can also drive the landward migration and eventual welding of nearshore bars along gently sloping shorefaces (Aagaard et al., 2004), and facilitate sediment transfers from the lower to the upper shoreface, thereby contributing to the nearshore sediment budget (Harley et al., 2022). These findings highlight the need for enhanced shoreface monitoring to enable accurate sediment budget assessments. Importantly, coastal dunes need to be also included in such analyses to achieve a comprehensive understanding of the cross-shore sediment system. Although beaches and dunes have traditionally been studied separately, early research highlighted the need to approach them as interconnected systems (Short and Hesp, 1982; Sherman and Bauer, 1993). Today, there is growing consensus that these systems are coupled, with significant sediment exchanges across the beach-dune boundary (Aagaard et al., 2004; Walker et al., 2017).

A lack of comprehensive perspective of the processes and sediment budget across the different compartments of the shore-beach-dune profile can prevent our ability to interpret the evolution of coastal systems. Coastal dunes are depositional landforms that rely on sediment supply from the beach, efficient wind events, and the establishment and growth of vegetation (Psuty, 1988; Hesp, 2002; Delgado-Fernández and Davidson-Arnott, 2011). Dunes exhibit considerable spatial variation in response to changes in sea-level (Davidson-Arnott and Bauer, 2021) and climatic drivers (Lancaster and Helm, 2000; Miot da Silva et al., 2013). Their morphology and vegetation communities often reflect changes in local sediment budgets (Psuty, 2004; Herrero et al., 2020; Moore et al., 2016), shoreline trends (DaSilva et al., 2024; Costas et al., 2023; Houser et al., 2008), vegetation types (Ruggiero et al., 2018), and human activities (Provoost et al., 2011; Delgado-Fernandez et al., 2019).

Dunes can advance seaward, increasing in width and height through foreslope accretion in pace with vegetation colonization and growth (Goldsmith, 1973; Hesp, 1988; Bristow et al., 2000), or by forming new crests in response to a positive sediment budget and active shoreline progradation (Psuty, 2004; Herrero et al., 2020). Conversely, dunes may undergo erosion during storm events, especially under conditions of rapid shoreline retreat and negative sediment budgets, leading to scarp formation and dune toe retreat (e.g., Masselink et al., 2022). Shoreline erosion can also trigger the formation of transgressive sand sheets that remobilize previously established sediment (Hesp et al., 2022; DaSilva et al., 2024), with landward transfers of sand facilitated by the formation of blowouts (Hesp, 2002; Talavera et al., 2024; Laporte-Fauret et al., 2022). Under conditions of positive or stable littoral sediment budgets, storms can lead to episodes of stoss slope dune erosion and dune toe retreat, followed by the formation of dune ramps that reconnect the upper beach with the dune, enabling landward transfer of sediment beyond the crest and dune crest migration (Ollerhead et al., 2013). This allows coastal dunes to move landwards, while maintaining their form and volume through sediment transfers from the stoss to the lee slope (Ollerhead et al., 2022; Davidson-Arnott et al., 2024). Notably, transgressive dunes may also occur in settings with high sediment supply and stable coastlines (Hesp, 2013), supporting the importance of assessing the sediment budget across the complete shore-dune-beach profile. This comprehensive approach is essential not only to understand dune state, but more importantly, to evaluate the broader state of the coastal system—whether it is stationary, regressive or transgressive. Such understanding is especially critical under ongoing and projected sea-level rise scenarios, which will largely determine coastal adaptation strategies.

Early studies defined coastal transgression as the mechanism by which siliciclastic coastal systems migrate landward when relative sea-level rise outpaces the influx of sediment (Curray, 1964; Fischer, 1961). Traditionally, transgression has been associated with coastal erosion or net loss of sediment from the subaerial beach to offshore or downdrift sediment sinks, leading to subsequent landward translation of the shoreline. Recent studies, however, suggest that transgression is not necessarily erosional. Beaches and barrier islands may migrate landward while retaining their volume, simply translating depositional environments inland—provided that adequate accommodation space is available (Houser, 2018; Kombiadou et al., 2019; Hein and Kirwan, 2024). Landward migration of barriers is facilitated through three main mechanisms (Cowell et al., 1995): overwash (Lorenzo-Trueba and Ashton, 2014), aeolian sediment transport (Costas, 2022), and barrier breaching (Leatherman, 1983; Nienhuis and Lorenzo-Trueba, 2019). While shoreline retreat due to sea-level rise typically unfolds over centennial to millennial timescales, the physical mechanisms that drive it—such as storm events and lower-energy wind-driven transport—occur on much shorter timescales (Masselink and van Heteren, 2014; Walker et al., 2017). This highlights the complex and often nonlinear response of coastal barriers to rising sea levels and storminess, and underscores the challenge of isolating the relative contributions of different drivers to barrier migration. These complexities further support the need for holistic approaches to analyzing coastal systems, particularly the coupled beach-dune system.

The El Niño-Southern Oscillation (ENSO) is the dominant driver of interannual climate variability across the Pacific Ocean, exerting a significant influence on the global climate (e.g., Oderiz et al., 2020). In northern Baja California, the highest winter wave energy occurs during the El Niño phase of ENSO, which causes the greatest coastal change (Ruiz de Alegría-Arzaburu and Vidal-Ruiz, 2018). Following the highly energetic 2015–2016 El Niño, shorelines along the sediment-starved California coast (USA) retreated beyond previously recorded landward extremes (Barnard et al., 2017). Comparable erosion occurred at Ensenada beach, where offshore sandbar migration beyond the cross-shore limit delayed subaerial recovery by three years (Vidal-Ruiz and Ruiz de Alegría-Arzaburu, 2020).

The aim of this study is to investigate how storms shape the evolution of transgressive coastal systems, specifically those featuring landward-migrating dunefields. To achieve this, we focus on the effects of El Niño winters, analyzing sediment exchanges across the entire nearshore-beach-dune profile. Focusing on a 1 km stretch of southern Ensenada beach in Baja California, Mexico, we assess El Niño's impact across three temporal scales: multidecadal, interannual and seasonal. This is done using satellite-derived shoreline data from 1984 to 2020 and sixty-six topo-bathymetric surveys conducted between 2014 and 2020. This study's objectives are: (1) to evaluate how El Niño events affect sediment exchanges and balance across the coastal profile; (2) to examine how these manifest over different time scales and influence long-term shoreline variability; and (3) to contextualize the observed dynamics in relation to the broader state of the coastal system (i.e., stationary, regressive or transgressive).

2. Research site

The field site is located at the southernmost 1.1 km of Ensenada Beach, within Todos Santos Bay, on the northwestern Pacific coast of the Baja California peninsula in Mexico (Figs. 1 and 2). The width of the beach and dunes changed significantly after the construction of the port and promenade in the early 1970s, during which most of the coastal lagoon was reclaimed for urban development. Today, "La Lagunita" is the only remnant of the former coastal lagoon (visible in Fig. 1, behind TB30). We conduct our research in this area (square section in Figs. 1c and 2).

The sand dunes in front of La Lagunita coastal lagoon (Fig. 2) present less than 15 % vegetation coverage (Carrillo–Rodríguez, 2016). Prevailing northwesterly winds are oblique onshore and relatively weak, with average speeds around 4 ms^{-1} (González-Yajimovich, 1981). In contrast, sporadic but more intense easterly (offshore) winds – known as Santa Ana winds – can exceed 10 $ms^{-1}$and reverse the dominant aeolian transport direction during the fall and winter.

The beach is made of medium sand (D_{50} = 0.25 mm) derived from intrusive rocks (Carriquiry–Beltrán, 1985) and is aligned north-to-south. It is exposed to west-northwesterly swell waves and is partly protected from the southern Pacific swell by the islands. The bathymetry of the bay is relatively shallow with depths of up to 50 m; however, a canyon with depths exceeding 400 m is present at the southern end of the bay (Fig. 1b). Incident waves are predominantly shore-normal due to wave refraction, but seasonal variations in the nearshore bathymetry

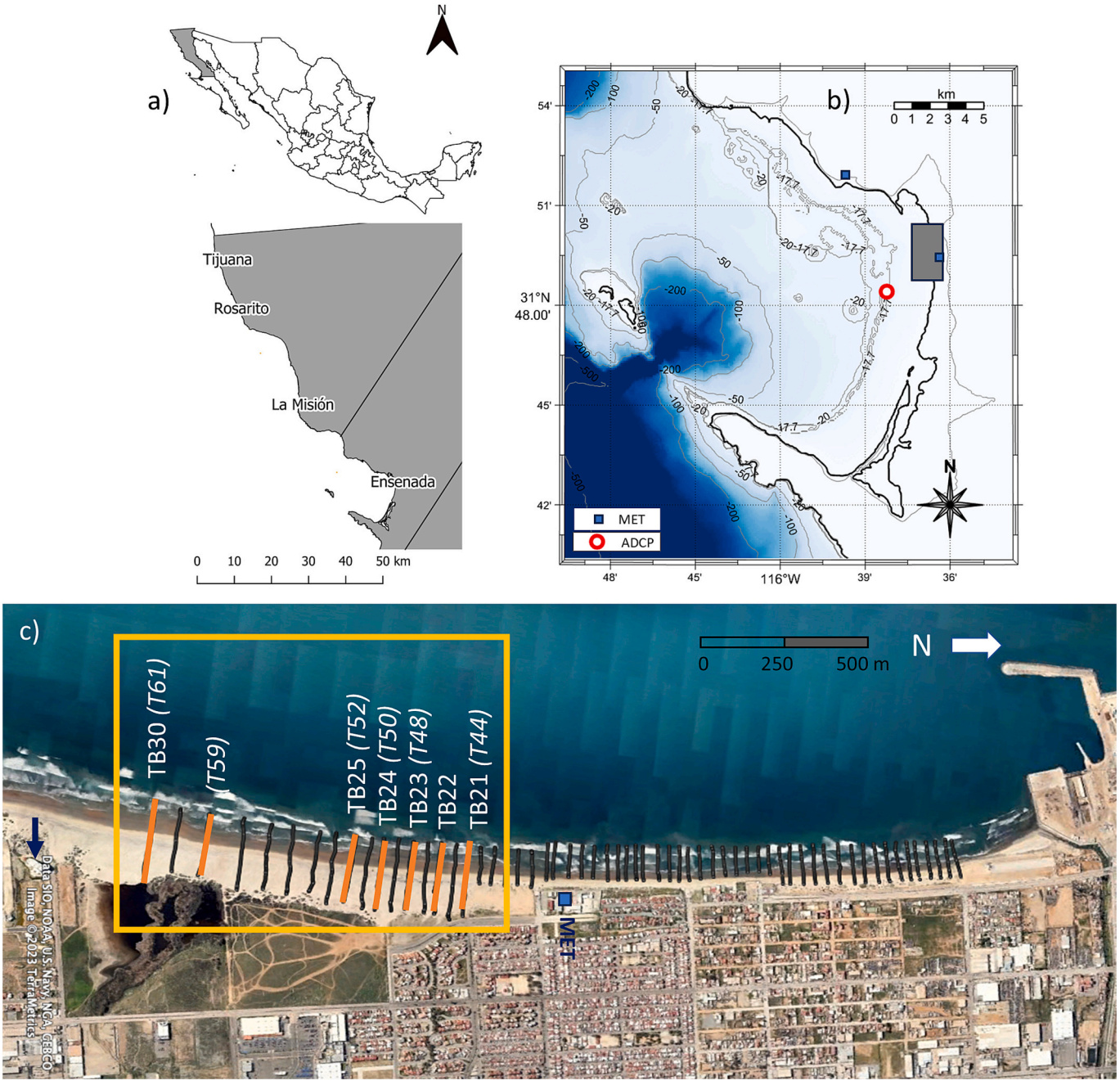

Fig. 1. (a) Location of Ensenada within the Baja California peninsula in Mexico. (b) Detailed bathymetry for Bahía Todos Santos; the location of Ensenada Beach in denoted in gray square (source: NOAA Digital Elevation Model). (c) Aerial view of Ensenada Beach. The orange square marks the research dune field site. Topo-bathymetric (TB) profiles analyzed in this study appear in orange, with corresponding topographic (T) shown in Fig. 3 in italics and inside brackets. The blue arrow points to the location of the Pacifica building (see Fig. 2).

Fig. 2. Aerial views from the study site: (a) Taken on June 1, 2013, from the roof of the Pacifica building (see arrow in b, and location in Fig. 1c); (b) Taken on January 6, 2023, with a UAV at high tide after a highly energetic storm. Image (a) faces north, while image (b) faces south.

contribute to longshore gradients in wave height. Low-energy conditions, characterized by shorter (T_p = 8 s) and smaller (H_s = 0.7 m) waves, occur between May and September. In contrast, longer (T_p = 12 s) and larger (H_s = 1.2 m) energetic waves are typical from October to April (Vidal-Ruiz and Ruiz de Alegría-Arzaburu, 2020; Ruiz de Alegría-Arzaburu et al., 2022). The astronomical tidal regime is semi-diurnal and micro-mesotidal, with a mean tidal range varying from 0.5 to 2.3 m across neap and spring tides, respectively (http://oceanografia.cicese.mx/predmar).

Changes in the morphodynamic beach state, as indicated by the dimensionless fall velocity ($\Omega = H_b/W_s\ T$; where H_b represents the height of breaking waves, W_s is the sediment settling velocity, and T is the wave period; Dean, 1973), reveal that reflective conditions prevail in spring and summer ($\Omega < 4$) with prevailing onshore winds, while dissipative conditions dominate in fall and winter when stronger sporadic offshore winds are likely to occur ($\Omega > 4$) (Vidal-Ruiz and Ruiz de Alegría-Arzaburu, 2020). Typically, cross-shore sediment transport outweighs the longshore. The annual cycle commonly involves berm erosion and sandbar formation during winter, followed by onshore sandbar migration in spring, and sandbar attachment to the shoreline along with berm rebuilding in summer (Vidal-Ruiz and Ruiz de Alegría-Arzaburu, 2019, 2020). The energetic swell waves, often exceeding heights of 3 m, that occur in winter drive the subaerial beach erosion (Ruiz de Alegría-Arzaburu et al., 2017). Significant morphological changes also occur across years, with the most severe erosion periods linked to successive swell storms during El Niño winters, characterized by low-pressure anomalies (Ruiz de Alegría-Arzaburu and Vidal-Ruiz, 2018).

3. Methods

3.1. Wave and wind data

Nearshore waves were measured hourly (17-min averages at 2 Hz) from August 2014 to October 2020 with an acoustic Doppler current profiler (ADCP; AWAC type from Nortek) located at an approximate depth of 18.5 m offshore from the southern end of Ensenada Beach (Fig. 1b). The instrument was moored on an aluminum pyramid and provided integral wave parameters including the significant wave height (H_s), spectral peak wave period (T_p), wave direction (Dir) and directional spreading. The hourly time series of six-years of wave data were used to calculate the total amount of wave energy transferred to the beach, the total wave power (P_t, Eq. (1)) through linear wave theory (Ruiz de Alegría-Arzaburu et al., 2022) as follows:

$$P_t = nEC \tag{1}$$

with n being the wave group to incident celerity ratio, $n = \frac{1}{2}\left(1 + \frac{4\pi d/L}{\sinh 4\pi d/L}\right)$; E the wave energy density, $E = \frac{1}{16}\rho g H_s^2$; C the wave celerity, $C = \frac{gT_p}{2\pi}\tanh\frac{2\pi d}{L}$; d the local depth; and L the wavelength.

Integral wave parameters and the total wave power were averaged between periods of morphological surveys, and the preceding wave parameters were compared to morphological variations. In addition, long-term hourly wave power data, calculated from integral wave parameters for the period 1984 to 2020, was derived using ERA5 wave reanalysis data (Hersbach et al., 2020) for the node closest to Ensenada (Lat = 31.5; Lon = −117). Wind measurements were collected from August 2014 to August 2019 with an automatic Vaisala meteorological station located at 10 m of elevation from mean low low-tide (MLLT) in the middle section of Ensenada Beach (see location in Fig. 1). Missing wind data from the local meteorological station for the 2014–2020 period were complemented with measurements from the CICESE meteorological station (https://observatorio.cicese.mx) located slightly inland and approximately 8 km north from the beach (see location in Fig. 1).

3.2. Morphological surveys and dune morphometrics

This study comprises sixty-six topographic and bathymetric surveys collected from August 2014 to October 2020, along a 2867 m section of the sandy coastline. Each beach survey consisted of approximately 50-m spaced 61 topographic (T) profiles and 100-m spaced 30 bathymetric (B) profiles extending typically up to 10 m of depth (Fig. 1c). Since the maximum depth monitored in some of the profiles was 8 m, this was the deepest limit considered for volumetric estimates. The Leica GS14 RTK GPS (real time kinematic Global Positioning System) was used to measure the topography with a vertical accuracy of a few centimeters. All profiles were measured on foot at a frequency of 1 Hz using a two-wheeled trolley operated by two people performing the survey down to MLLT (+36.135 m from ellipsoidal heights), and a threshold value of 0.05 m was established to discard erroneous data during post-processing. Bathymetric profiles were measured using a jetski equipped with the 0.5 MHz echo-sounder integrated in the Sontek Hydrosurveyor ADCP synchronized to an RTK-GPS antenna.

A total of 30 topo-bathymetric (TB) profiles were collected per survey, with TB1 positioned at the northernmost point of Ensenada Beach and TB30 at the southernmost point (Fig. 1c). For this study, only the southernmost profiles —TB21–25 and TB30—were analyzed, as they were the only ones that included the complete topography across the dune ridge. Some profiles, such as TB21 and TB30, began on a flat surface, while the others included presented additional dune crests

further landward. As a result, sand can migrate onshore, and the sediment budget is not necessarily closed within each profile. Throughout the study period, the dune toe was not reached by marine processes; therefore, this area— like the dune itself—is considered predominantly aeolian.

The morphological evolution of the beach was assessed by analyzing changes in each TB profile over time. Volumes (m^3m^{-1}) were calculated for different sections —subtidal (Z < 0 to −8 m), intertidal (Z > 0 to 2 m), supratidal (Z > 2 to 4 m), dune toe (Z > 4 to 4.5 m), and dune (Z > 4.5 m to Zmax)—by integrating upwards from specific elevations. To evaluate the volumetric evolution of each beach section over the six-year study period, instantaneous volumes were de-meaned and cumulatively assessed. Dune crest cross-shore positions (X_d) and elevations (Z_d) were manually extracted from each linearly interpolated TB profile (TB21—25 and TB30) at 0.1 m cross-shore intervals. Stoss slopes were calculated for the elevation range between 4.5 m and 6 m, while lee slopes were determined from the minimum elevation (Z min) of the initial profile up to 7.5 m, near the crest.

3.3. Long-term satellite-derived shorelines and validation

Time series of satellite-derived shoreline (SDS) positions were retrieved for the locations of measured profiles TB21—25 and TB30 (source: http://coastsat.wrl.unsw.edu.au). SDS were obtained from the CoastSat toolkit developed by Vos et al. (2019a, 2019b) from publicly accessible optical satellite data via Google Earth Engine, specifically Landsat 5, 7 and 8 with a spatial resolution of 30 m, as well as Sentinel-2 images with a finer 10-m spatial resolution. In essence, CoastSat uses a Neural Network classifier to categorize RGB (+ infrared) satellite images into four distinct classes. Coupled with a global threshold on the Modified Normalized Difference Water Index (MNDWI), it then employs a sub-pixel resolution contouring algorithm to derive a waterline from the image. For further details on CoastSat refer to Vos et al. (2019b).

At each transect, time series of shoreline deviation from the mean was retrieved from SDS. For SDS validation topographic measurements were used. Topographic data of eight years (2012 to 2020) for the locations of TB21–25 and TB29–30 were used (Fig. 1). A total of 101 in-situ shorelines were extracted from this dataset as the intersection of the beach profile with elevation Z = 1 m, a close reference to the mean tide level (MTL; Z = 0.82 m). The comparative time-series of measured (topography-derived) and SDS (CoastSat-derived) shoreline positions between November 2012 and October 2020 for TB21 (T44), TB23 (T48), TB24 (T50), TB25 (T52), TB29 (T59) and TB30 (T61) demonstrate close agreement between the two datasets (Fig. 3). Thus, SDS from 1984 to 2020 were used to analyze long-term beachface variations in the past four decades.

4. Results

4.1. Long-term shoreline variability 1984–2021

Multi-decadal variations reveal that the shoreline is shifting toward land, reflecting the transgressive nature of the field site. From 1984 to 1997, shorelines showed relative stability around their average location. However, the highly energetic El Niño 1997–1998 (see peak in Fig. 4b) triggered a recession that persisted over the following decades, exacerbated by subsequent El Niño events (Fig. 4a, c). Notably, shoreline retreats were more pronounced during intense El Niño events (ONI > 1.5). Under high-energy conditions (monthly average P_t > 30 kW/m) the shoreline typically retreated 20 m below the average position, while it generally accreted to 20 m above average during low-energy conditions (monthly average P_t < 15 kW/m), (Fig. 4b, c).

Overall, the shoreline exhibited a similar response across the 1-km stretch of beach, with seasonal shifts of ±20 m in response to wave energy. Shoreline advancements typically occurred in summer, while retreats in winter (see gray lines in Fig. 4c). The widest beach widths in

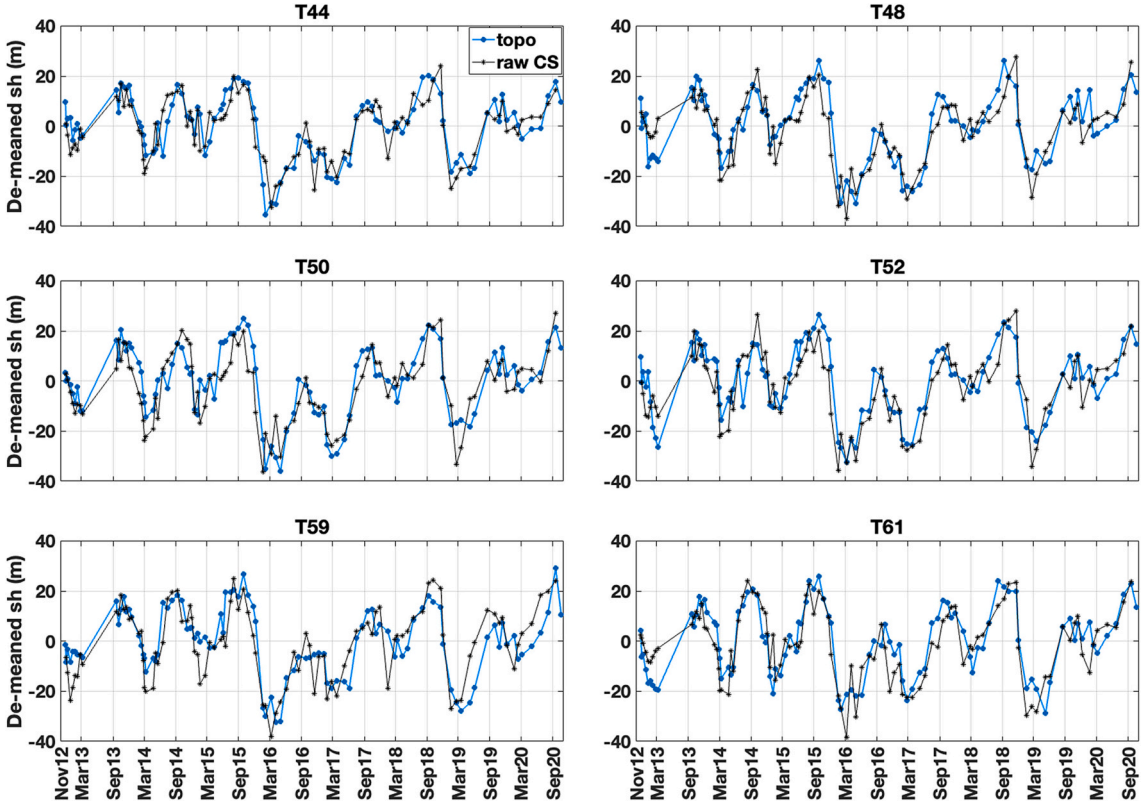

Fig. 3. Time-series of de-meaned measured (blue circles; Topo) and CoastSat-derived (black stars) 1-m shoreline variations between November 2012 and October 2020 for transects T44 (TB21), T48 (TB23), T50 (TB24), T52 (TB25), T59 (TB29) and T61 (TB30; north to south) in Ensenada Beach (see locations in Fig. 1c).

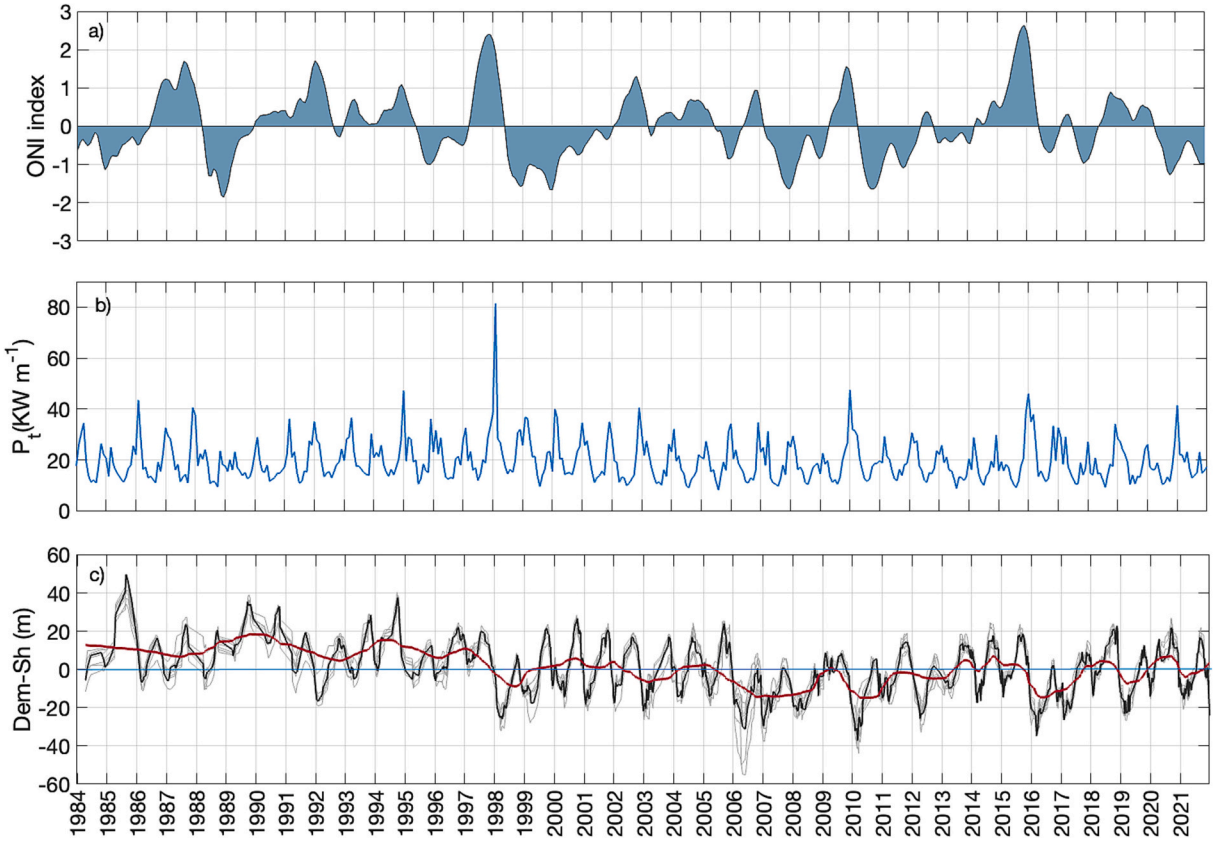

Fig. 4. Time-series from 1984 2021 of: (a) Oceanic Niño Index (ONI); (b) Monthly average total wave power (P_t); and (c) raw de-meaned and smoothed SDS for TB21–25 and TB29–30 (gray lines), and the average shoreline (black line). The red line represents the 5-year average de-meaned shoreline trend. Positive ONI and negative Dem-Sh values indicate El Niño conditions and shoreline recession relative to the mean, respectively.

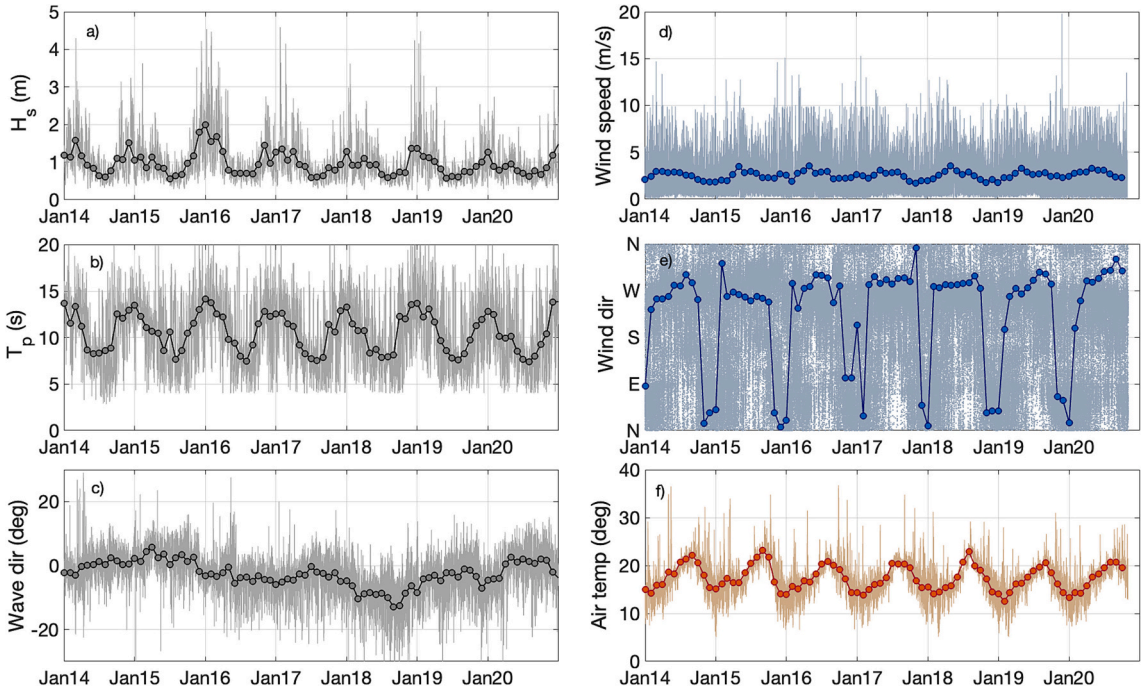

Fig. 5. Time-series of hourly wave data and 10-min meteorological data for Ensenada from 2014 to 2020: (a) significant wave height, H_s; (b) spectral wave period, T_p; (c) wave direction; (d) wind speed; (e) wind direction (West = onshore; East = offshore); and (f) air temperature. Monthly-averaged values are shown in dots for each variable.

the study period (maximum de-meaned shorelines) occurred in 1985, prior to El Niño 1986–1987. The 5-year average trend (red line in Fig. 4c) indicated above-average shorelines before El Niño 1997–1998. Since then, shoreline positions have oscillated around the long-term mean, with minimum values associated with energetic El Niño 2009–2010 and 2015–2016 (Fig. 4). The long-term shoreline trend calculated from the 5-year average showed an approximate average retreat of 0.3 m/yr over the 37 years (1984–2021), and an accelerated retreat of 1.7 m/yr in the period 1984–1998. Although this study does not explicitly analyze vegetation cover, the period of exacerbated shoreline recession appears to coincide with a decline in vegetation, as discussed in Section 5.

4.2. Wave and wind characteristics

Nearshore wave conditions in Ensenada exhibit distinct seasonality (Fig. 5a, b, c). During winter, significant wave heights (H_s) can reach 4.5 m with periods up to 22 s, while in summer, wave heights are typically below 1 m with periods shorter than 10 s. Waves are predominantly shore-normal (0° in Fig. 5c), with minimal directional variation due to wave refraction. Monthly-averaged wave heights peak around 1.5 m in winter and 0.6 m in summer (circles in Fig. 5a).

Interannual variability in wave conditions is evident during El Niño years. During the very strong 2015–2016 El Niño winter (Fig. 5a, b), waves were more energetic than in other winters; monthly-averaged H_s exceeded 1.5 m from December to March, reaching 2 m in January. In contrast, the moderate 2018–2019 El Niño event presented several winter storms with H_s surpassing 4 m, but monthly-averaged H_s did not exceed 1.5 m (Fig. 5a).

Wind speeds generally reach up to 10 ms^{-1} (10-minute averages), with monthly means ranging from 3 to 4 ms^{-1}. Winds are predominantly onshore, from the WWS-W and NW, between February and October, and shift to offshore, from the NNE-NE, from November to January (Fig. 5d, e). While the dominant wind direction was from the WWN in most years of this study, winds from the WWS prevailed between 2014 and 2016. Air temperature also shows marked seasonal variation, with monthly

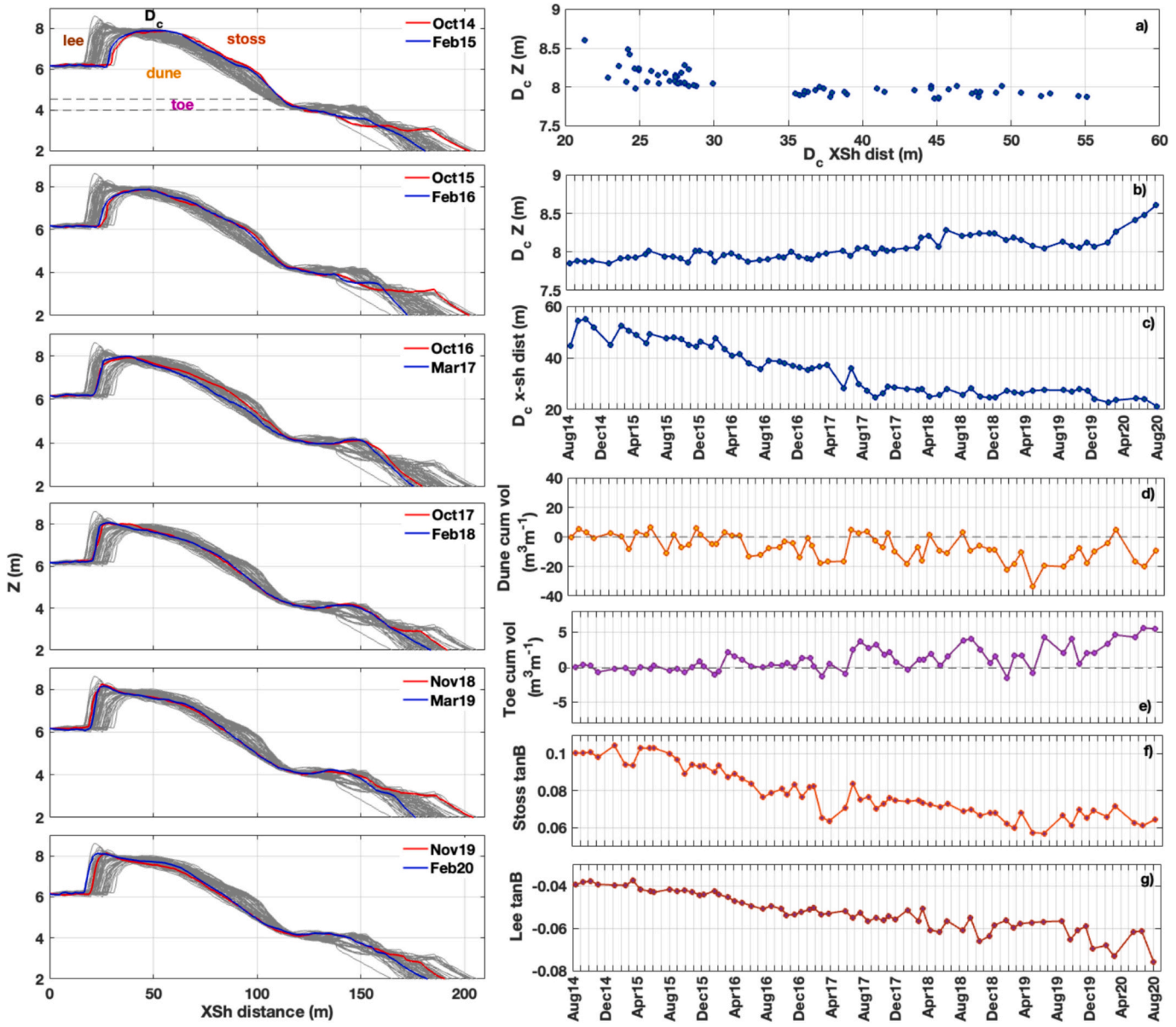

Fig. 6. Left panels show morphological dune evolution at TB21 highlighting summer (red) and winter (blue) changes. Right panels show: (a) dune crest (D_c) elevation and cross-shore variations; (b) time-series of D_c elevation and (c) cross-shore variations; (d, e) time-series of cumulative volume differences for the dune and dune toe zone; and (f, g) time-series of stoss and lee slope (tanB) variations.

averages ranging from 15 °C in January to 23 °C in September. The minimum and maximum recorded temperatures during the study period were 6 °C and 36 °C, respectively (Fig. 5f).

4.3. Dune morphodynamics

Significant differences in dune morphodynamics were evident alongshore (Figs. 6 and 7). As an example of the morphological variations of the dune, the northernmost profile TB21, showed a significant landward migration of the crest (D_c) by 34 m over the six-year period (Fig. 6c), along with an increase in height from 7.8 to 8.6 m (Fig. 6a, b). During this time, the stoss slope flattened from tanβ 0.1 to 0.06 (Fig. 6f) while the lee slope steepened from tanβ 0.04 to 0.08 (Fig. 6g). The dune in this profile experienced erosion of 8 m^3/m between 2014 and 2020, with specific erosive periods following high-energy wave events (e.g., April–June 2016, Jan–Feb 2017, Nov 2017–Jan 2018, Dec 2018–Mar 2019; Fig. 6d), when the subaerial beach was notably eroded (Fig. 8).

In the dune toe zone, volume evolution indicated a positive trend, with a net gain of 5 m^3/m, showing similar fluctuations to those of the dune over the study period (Fig. 6d, e). The largest onshore D_c migrations occurred from August 2014 to 2017, during which both dune and toe volumes remained relatively stable (Fig. 6c). However, significant fluctuations in dune volume were observed in the final two years, with April 2019 to March 2020 being a period of notable dune recovery (+30 m^3/m Fig. 6d), coinciding with accretion in the dune toe zone (+5 m^3/m Fig. 6e). From March to June 2020, the dune lost 20 m^3/m, while D_c height increased by more than 0.5 m (Fig. 6b, d).

Dune crests varied alongshore in both position and elevation (see upper panels in Fig. 7). In TB21 and TB23, flatter mobile dunes with elevations below 9 m (Fig. 7a1, a3) exhibited a single crest that gradually migrated landward between 22 and 35 m (Fig. 7b1, b3). TB22, located between these profiles, featured a slightly higher dune crest with similar net landward migration of 22 m (blue dots in Fig. 7a2, b2). However, it also developed an incipient dune that migrated 26 m landward, merging with the primary crest by September 2017 (red dots in Fig. 7b2). By February 2018, the primary crest split into two: the landward crest continued migrating onshore (light blue dots in Fig. 7b2), while the primary crest position stabilized seaward until

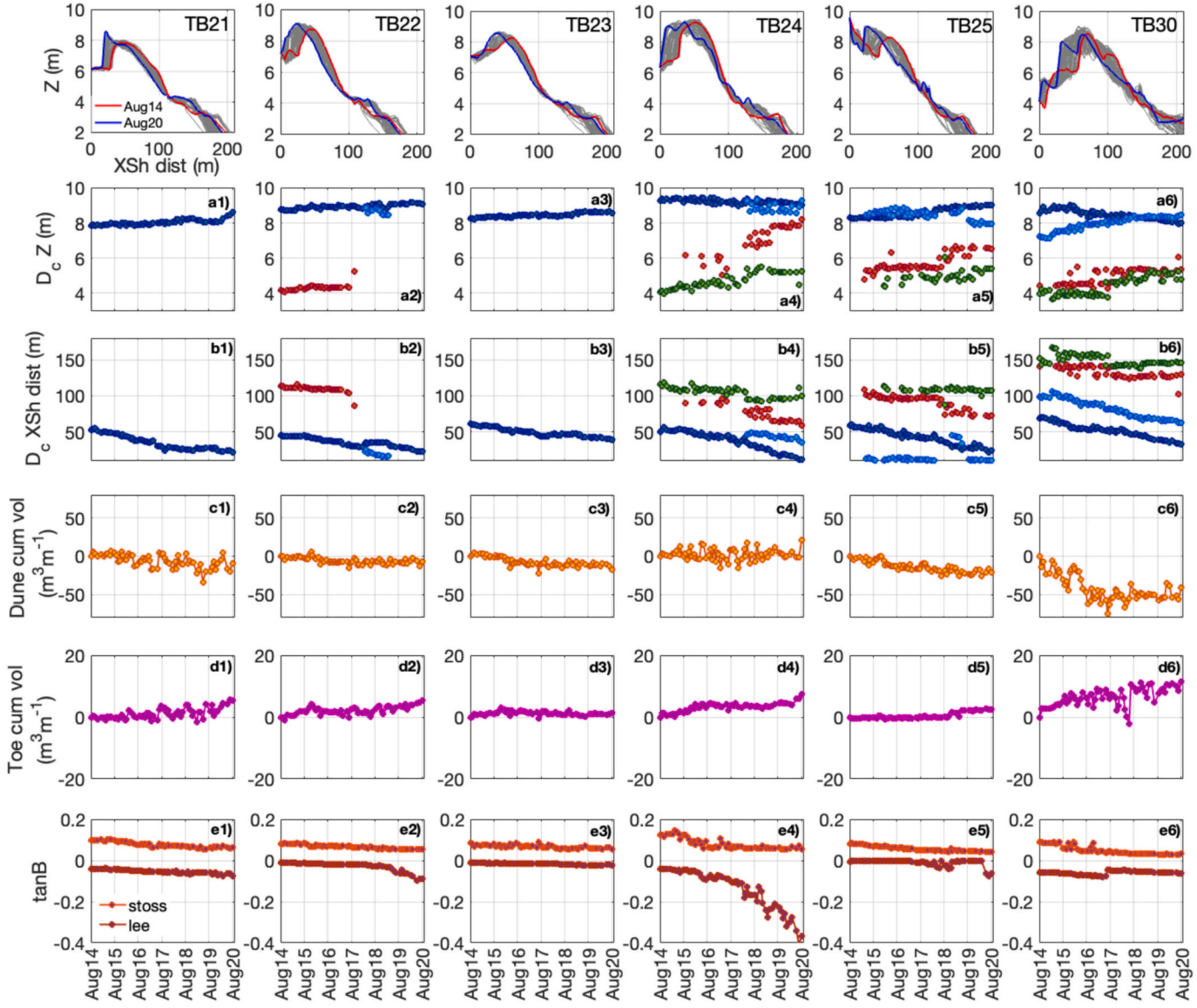

Fig. 7. Upper panels: supratidal and dune morphological evolution for TB21–25 and T 30 from August 2014 to October 2020. Time-series of: (a) dune crest elevation (D_c Z); (b) Cross-shore dune crest position from the upper beach (D_c XSh); (c, d) Cumulative differences of volumes for the dune and toe sections; (e) stoss and lee slopes (tanB) in orange and dark red, respectively.

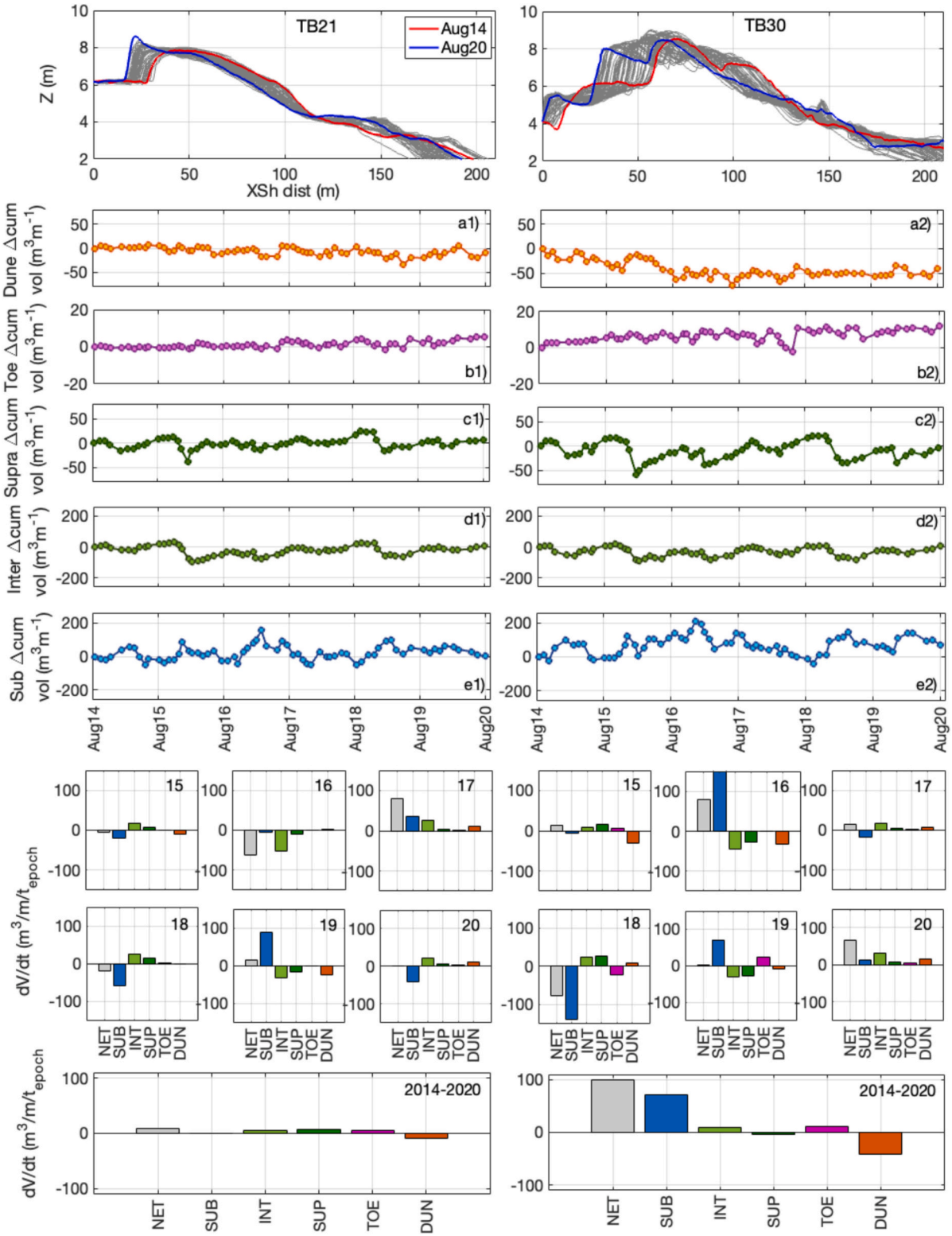

Fig. 8. Morphological changes of profiles TB21 and TB30 for the supratidal beach to the dune. Panels a-e show the time series of dune, toe, supratidal, intertidal and subtidal cumulative volume changes from August 2014 to 2020 for TB21 (1) and TB30 (2). The bottom histograms present the sediment balance for each beach section and year (15–20) for TB21 (left) and TB30 (right). The bottommost panels indicate net volume changes for each beach section and profile for the 2014–2020 period.

February 2019, when both merged again (blue dots in Fig. 7b2). In these three profiles (TB21-TB23), dune volumes decreased 10 to 20 m^3/m over the time (Fig. 7c1–c3), while dune toe volumes showed increasing trends but of smaller magnitude of up to 5 m^3/m (Fig. 7d1–d3). Stoss slopes decreased while lee slopes increased (Fig. 7e1–e3), and the lee slope steepened the most in TB22 after the 2018–2019 El Niño winter (Fig. 7e2).

Main dune crests migrated 36–40 m landward further south in TB24,

TB25 and TB30, where crests were wider and/or higher than further north (dark blue dots in Fig. 7a, b). These profiles exhibited one or two incipient crests (green and red dots), as well as primary (dark blue dots) and secondary (light blue dots) crests further inland. In TB24, the secondary crest developed after February 2018, when incipient dunes migrated landward, which coincided with a landward shift of the main crest (Fig. 7a4, b4). In TB25, incipient crests (green and red dots) also contributed to the formation of a secondary crest (light blue dots) by the end of 2018 (Fig. 7a5, b5). This secondary crest initially formed in April 2015, located 40 m landward relative to the main crest, and remained relatively stable throughout the study period, except between February 2018 and August 2019, when it temporarily merged with the main crest (Fig. 7b5).

The southernmost profile, TB30, wider profile than the others, showed primary and secondary crests 30–35 m apart that migrated 36–42 m landward during the study period (blue dots in Fig. 7a6, b6). Incipient dunes also migrated onshore and welded the main ridge at specific times (red dots, Fig. 7a6, b6). While TB25 exhibited similar trends in dune and toe volumes as the northern profiles TB21–23 (Fig. 7c5, d5), the southernmost profile, TB30, experienced substantial dune erosion of 50 m^3/m from August 2014–2016— since it is not a closed profile, part of this apparent loss may be due to inland transfer— stabilizing after August 2016 (Fig. 7c6). The toe volume for TB30 increased by 10 m^3/m almost linearly throughout the study period (Fig. 7d6). In contrast to the other profiles, TB24 presented an accretive trend in dune volume of 15 m^3/m, along with a 7 m^3/m increase in toe volume (Fig. 7c4, d4). This profile exhibited a pronounced steepening of the lee slope (Fig. 7e4) compared to other profiles.

4.4. Cross-shore sediment exchange

The cross-shore sediment exchange from the upper-shoreface to the dune for the northernmost and southernmost profiles, TB21 and TB30, showed minimal net changes in all years, except during El Niño events (calculated from August to August; see histograms in Fig. 8). In TB21, a negative net volume occurred in 2015–2016 (see 16 in Fig. 8), which was compensated by gains the following year (see 17 in Fig. 8), resulting in almost zero net change over the six-year period (+10 m^3m^{-1}). In contrast, TB30 exhibited much larger annual variations. Net sediment gains of 80 m^3/m occurred during 2015–2016 (see 16 in Fig. 8) due to

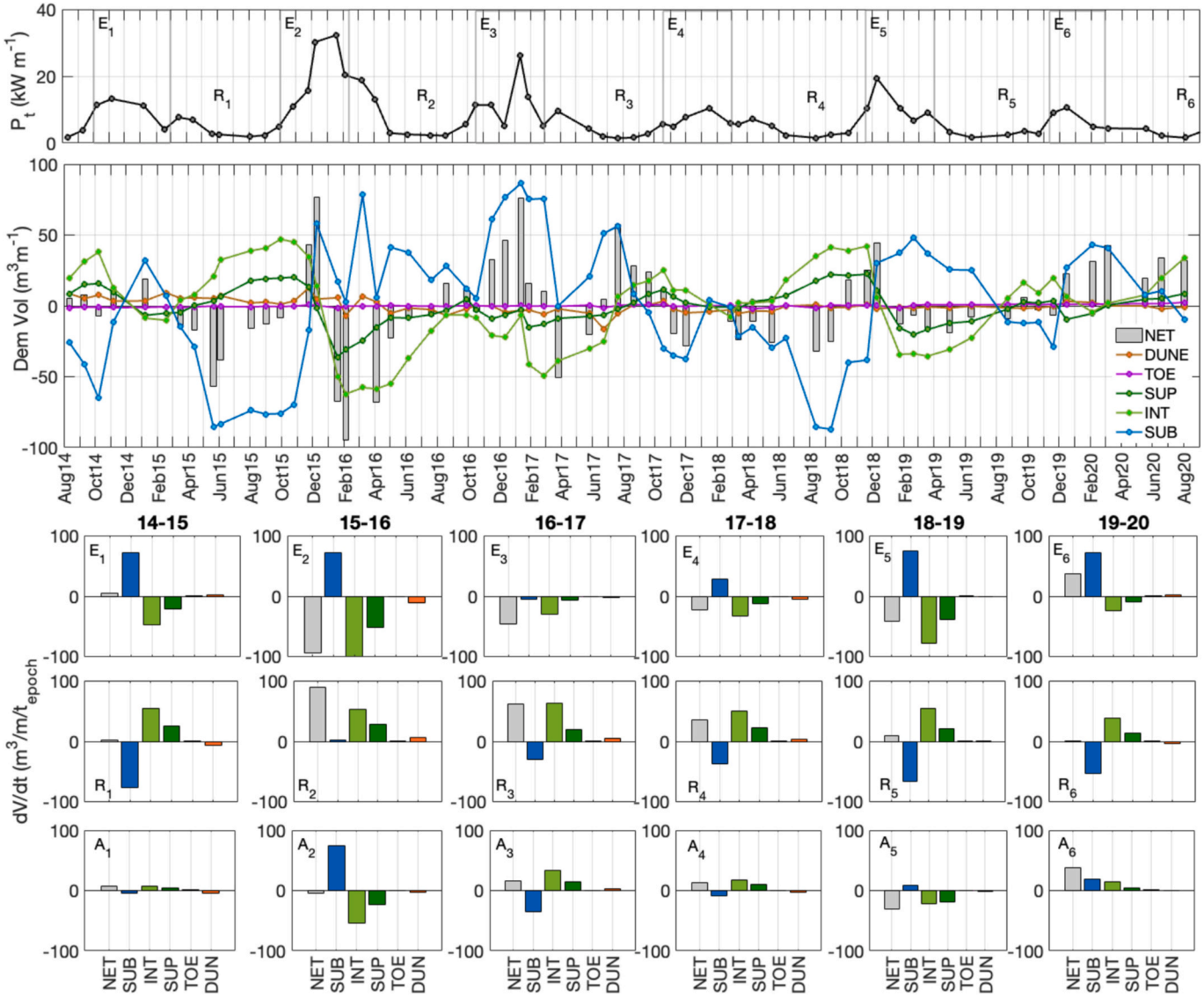

Fig. 9. Top panel: time-series of the total wave power averaged per survey periods (P_t). Middle panel: time-series of de-meaned volumes for the dune (orange), toe (magenta), supratidal (dark green), intertidal (light green), subtidal (blue) and total net changes (gray bars). Bottom panels represent sediment balances per period of time, erosive (E) and recovery (R) periods, and annual changes (A) for the six-years (1 to 6).

significant subtidal sediment inputs, while large subtidal erosion led to a negative balance in 2017–2018 (see 17 in Fig. 8).

Although TB21 experienced 22 m of D_c retreat, migration in TB30 was nearly double, reaching 42 m. Additionally, while dune volume remained relatively stable in TB21, it significantly decreased in TB30, despite an increase in dune toe volume. As indicated before, this could be due to inland transfer, as TB30 is not a closed profile (Fig. 8a, b). Over the study period, both profiles displayed similar seasonal intertidal and supratidal volume variations, with minimum volumes in winter (January to March) and maximum volumes in late summer and fall (September to November) (Fig. 8d and c). However, supratidal seasonal variations were more pronounced in TB30 compared to TB24 (Fig. 8c1, c2). Subtidal volume changes were also larger in TB30, particularly after the El Niño winters 2015–2016 and 2018–2019 (Fig. 8e1, e2), when the subaerial beach remained eroded (Fig. 8c, d).

4.5. Sediment balance

The volumetric sediment balance was calculated along the entire site length of 1142 m, spanning from TB21 to TB30 and including subtidal, intertidal, supratidal, toe, and dune areas (Fig. 9). Notably, during the study period, the dune and toe area remained primarily influenced by aeolian processes, as waves did not reach those elevations.

During high-energy conditions ($P_t \geq 15$ kWm^{-1}) associated with El Niño 2015–2016, the energetic winter 2017, and El Niño 2018–2019—corresponding to E_2, E_3 and E_5 in Fig. 9—net sediment losses ranged between 40 and 90 m^3/m (gray bars in E, Fig. 9), primarily due to subaerial beach erosion (green bars in E, Fig. 9), as sand was transported offshore. In contrast, during low-energy ($P_t < 15$ kWm^{-1}) recovery periods, erosion typically occurred in the subtidal zone (blue bars in R, Fig. 9) while the subaerial beach (intertidal and supratidal areas) gained sediment (green bars in R, Fig. 9), indicating onshore transport.

Throughout most years, sediment recovery during lower-energy

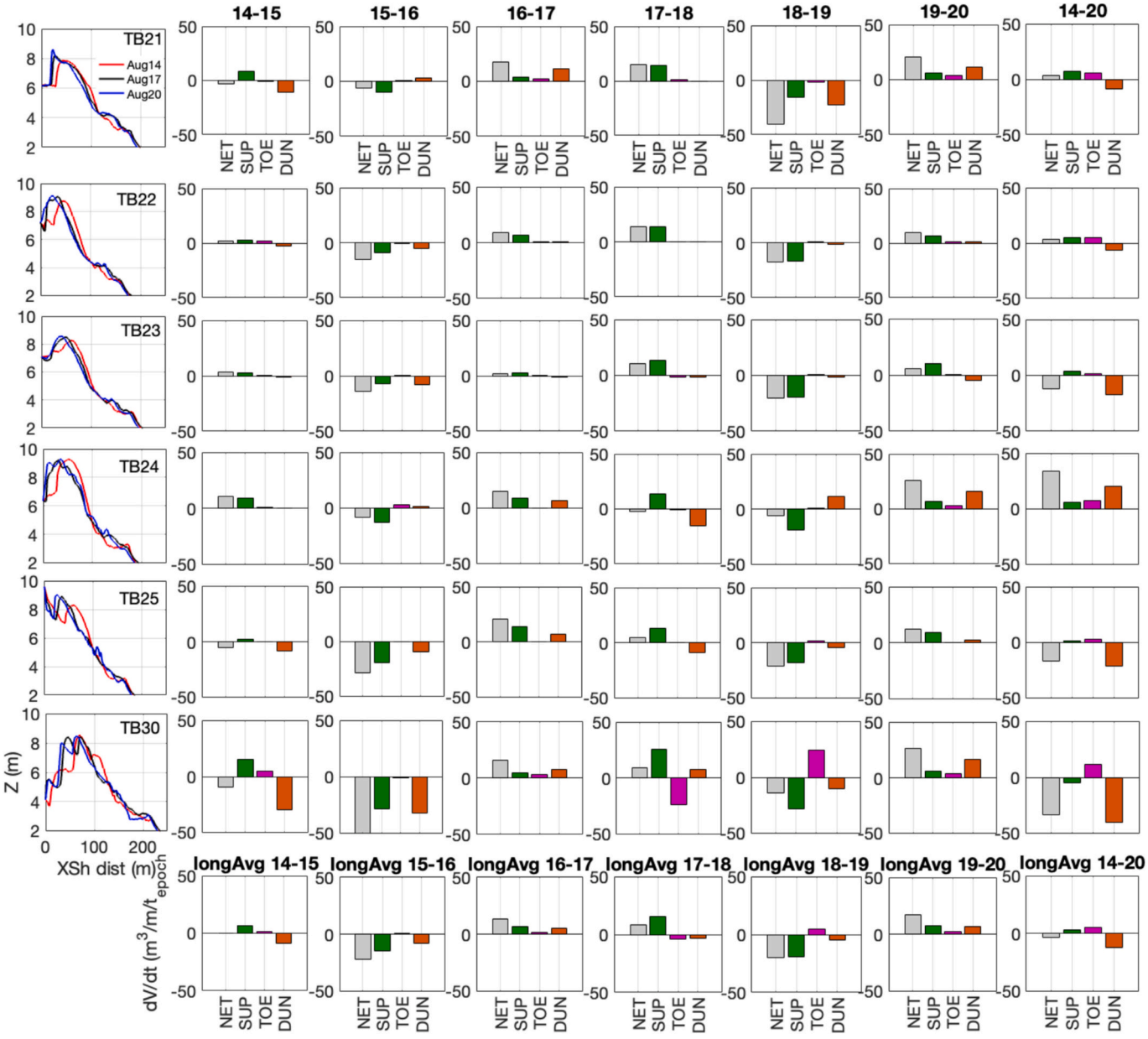

Fig. 10. Volumetric balance for the supratidal (green), toe (magenta), and dune (orange) sections from TB21 to TB30 (top to bottom) across different years. For example, '14–15' indicate the difference between August 2014 and August 2015. The bottom panels show the longshore-average results for each period of time.

periods compensated for the losses sustained in winter. Net annual variations in sediment balance fluctuate up to ±30 m^3/m (gray bars in A, Fig. 9), with net gains observed in the years following El Niño (A3, A4, and A6 in Fig. 9). The beach recovered its sand volume after the 2015–2016 El Niño and even presented a surplus of 38 m^3/m during the low-energy year following the 2018–2019 El Niño (net in A, Fig. 9). Volume changes in the dune were comparatively small; it eroded by 10 m^3/m during the most energetic period of the El Niño 2015–2016 (E_2 in Fig. 9), but annual variations remained subtle, at approximately ±3 m^3/m (orange bars in A, Fig. 9).

To specifically analyze alongshore variations in sediment exchange from TB21 to TB30 and among the supratidal, toe, and dune areas, a volumetric balance was conducted (Fig. 10). Over the six-year period from 2014 to 2020, the net longshore average volume change was close to zero, with a dune volume loss of 10 m^3/m (longAvg 14–20, Fig. 10), which, as mentioned earlier, may be related to inland sediment transfer. Annual longshore average volumetric balances showed net losses during El Niño years (e.g., longAvg 15–16 and 18–19, Fig. 10), primarily due to supratidal beach erosion. In contrast, the years following El Niño events (longAvg 16–17 and 19–20, Fig. 10) exhibited positive volume changes of approximately 7 m^3/m in the dunes, coinciding with supratidal beach recovery and overall net gains.

Overall, net negative volume changes and dune erosion occurred during the energetic El Niño 2015–2016 (Fig. 10), while dune volume gains and positive net changes were observed in the years following El Niño events (2016–2017 and 2019–2020, Fig. 10). The northernmost profiles (TB21 and TB22) showed similar six-year trends, with modest gains in the supratidal and toe area (6 m^3/m each), offset by dune volume losses of comparable magnitude (Fig. 10). TB23 followed a similar pattern but experienced a net negative annual balance and a total dune volume loss of 15 m^3/m over the six-year period (Fig. 10).

Southward alongshore, volumetric changes became more pronounced, especially during the erosive El Niño years. The southernmost profiles (TB25 and TB30) exhibited consistent net volume losses and dune erosion from 2014 to 2020, marked by significant erosion during El Niño events and accretion in the subsequent years (Fig. 10). TB30 recorded the largest dune sediment loss of 30 m^3/m/yr between 2014 and 2016, followed by a modest recovery of 8 m^3/m/yr from 2016 to 2018, another erosion phase of 9 m^3/m during the 2018–2019 El Niño, and accretion of 16 m^3/m in 2019–2020. The net dune volume change at TB30 over the six-year period was a loss of 40 m^3/m (Fig. 10), possibly transferred inland. In contrast, profile TB24—characterized by the steepest dune—diverged from the overall trend, showing a net gain of 35 m^3/m and a dune volume increase of 22 m^3/m over the study period (Fig. 10).

5. Discussion

5.1. The role of ENSO

Across the Pacific Basin, interannual climate variability is primarily governed by the El Niño–Southern Oscillation (ENSO), which induces significant shifts in oceanographic conditions that impact coastlines. The Eastern Pacific is especially vulnerable to erosion during strong El Niño phases, as was evident during the 1997–1998 event (Vos et al., 2023). This event included extreme storms that generated waves exceeding 10 m off Baja California (Storlazzi et al., 2000) and caused major sea-cliff retreat along the Central California coast (Sallenger Jr et al., 2002), as well as extraordinary subaerial beach erosion in Rosarito, northern Baja California (Lizarraga-Arciniega et al., 2003). In Ensenada, multi-decadal shoreline variations reveal that the powerful 1997–1998 El Niño shifted the long-term shoreline to a new landward position, reflecting a stepwise long-term recession indicative of the transgressive behavior of the beach. The major storms during the exceptional 1997–1998 El Niño can be compared to the impact of a hurricane, which can drive landward sediment transport across barrier islands and deposition of washover deposits (Rodríguez et al., 2020), ultimately causing the shoreline to migrate landward to a new average position. Comparatively, subsequent energetic El Niño events—such as the 2015–2016, which exhibited roughly half of the wave power of the 1997–1998—did not produce similar widespread erosion (Vos et al., 2023), and the subaerial beach—shoreline position—recovered within a few years (Ruiz de Alegría-Arzaburu and Vidal-Ruiz, 2018).

In the shorter-term (2014–2020), Ensenada exhibited a relatively stable shoreline trend (retreat of ~0.3 m/yr), characterized by seasonal fluctuations around an average position. However, during this same period, the dunes showed evidence of transgression (landward migration of 5 m/yr)—consistent with observations in other regions in the context of rising sea levels and storminess (Hesp et al., 2022; Hein and Kirwan, 2024)—though not necessarily associated with erosion (Ollerhead et al., 2013). In Ensenada, the absence of vegetation combined with predominant onshore winds result in net landward dune ridge migration. Despite this, sediment from the winter-berm is transported onshore as bedload features that roll upslope. Additionally, sediment is supplied from the subtidal section, particularly following El Niño events. These two sediment sources contribute to the formation of new incipient dunes on the back-beach. Depending on their location, these newly formed dunes may either remain isolated or eventually merge with existing ones. As mature dunes migrate inland and become progressively decoupled from the active beach, new, smaller dunes continue to form behind them, sustaining a dynamic system that gradually transfers sediment and advances inland.

The horizontal and vertical position of the dune toe is strongly influenced by frontal dune erosion (Castelle et al., 2017), sediment availability (Costas et al., 2016), aeolian processes (Walker et al., 2017) and sea-level (Davidson-Arnott, 2005; Burvingt and Castelle, 2023). This article identifies the dune toe at an elevation of 4.0–4.5 m, representing a vertical range of 0.5 m which may not always coincide with the base of the stoss slope of a traditional foredune. Furthermore, in their analyses of inconsistencies in dune toe definitions, Smith et al. (2020) reported considerable variability in the identification of foredune toes, depending on the type of imagery used and the level of user expertise. Despite these limitations, this study treats the dune toe as a distinct morphological area to describe its behavior at Ensenada. This zone functioned as a "bypass area", where a progressive decoupling occurred between the beach and the mobile dunes migrating landward. At times, it also served as a zone for the formation of new incipient dunes, that tended to migrate landwards too. It is important to note, however, that because waves did not reach the dune toe during the study period (see Section X), dune toe volumes could be merged with dune overall volumes and considered part of the "aeolian component" of the transect.

In vegetated shorelines subject to rising sea-levels, dunes may not keep up if local sediment budgets are negative. However, provided stable to positive sediment budgets and appropriate accommodation space, empirical evidence suggests that storms can push the dune toe landwards and upwards via wave scarping of dune stoss slopes. This temporarily kills dune vegetation in the dune toe area, with the subsequent formation of an unvegetated sand ramp that facilitates sediment transfers toward the dune crest and lee side (Davidson-Arnott et al., 2018; Ollerhead et al., 2013; Costas et al., 2023). This mechanism allows vegetated sand dunes to migrate landwards and upwards with rising sea-levels (Davidson-Arnott and Bauer, 2021). In the case of Ensenada, the dunes are sparsely vegetated, which facilitates the free movement of sand by wind throughout the year and across the dune profile; as a result, coastal dunes tend to move inland "as a block". Sequential analysis of satellite imagery suggest that dune movement is triggered by subaerial beach erosion, inundation, and aeolian deflation. The dune toe remained unaffected during extreme water levels and dune transgression took place without scarp formation.

5.2. Beach-dune sediment balance

The beach-dune sediment balance aims to account for the amount of sand delivered to the dune from the beach versus the amount carried inland. In many coastal regions, transgressive dunefield development is associated with marine sediment erosion (Roy et al., 1980; Hesp, 2013; DaSilva et al., 2024). In Ensenada, dune dynamics are primarily driven by aeolian processes. Inland dune migration is facilitated by onshore winds and the absence of vegetation cover. A small fraction of the dune volume is likely lost from the main ridge by winds that carry it further inland. The dunes migrate inland at a faster rate than the beach is retreating, suggesting a decoupling from the beach system. However, a one-way coupling exists between the dunes and the winter-berms. These elevated features—often preserved beyond the reach of regular wave activity—serve as sediment sources that are mobilized by wind to form incipient dunes. Aagaard et al. (2004) also describe an onshore sediment transfer pathway, from the subtidal zone to the intertidal beach and subsequently to the dunes and foredunes. In Ensenada, winter-berms play a key role in this sediment exchange, facilitating the wind-driven transport of sand from the beach to the dune. Although sediment inputs from the supratidal winter-berm to the dune toe partially compensate for inland sand losses, an alongshore average sediment leakage of approximately 10 m^3/m occurred over the six-year study period.

The rate of sediment supply to the coastal budget is a key factor influencing shoreline change along active, open-ocean coasts, ultimately controlling the pace of transgression (Hein and Kirwan, 2024). In Ensenada, the net sediment volume shows a positive balance of +40 m^3/m over the 2014–2020 period, primarily due to inputs from the subtidal section. Although the dunes migrate inland, they maintain a relatively stable sediment balance within a one-way coupled system. The upper beach, however, recovers its volume through inputs from the subtidal section. Thus, as long as sediment inputs from offshore (i.e., lower shoreface) or alongshore sources persist, this beach segment can continue to offset sand losses to the dune. These findings suggest that the shallow shoreface of Todos Santos Bay (average depth of 30 m) may hold sand deposits from past highly-energy erosional events—such as the 1997–1998 El Niño—that could be remobilized and transported onshore under certain conditions, contributing to the beach sediment budget (Harley et al., 2022). This dynamic may support temporal stability in the beach's transgressive trend (Hein and Kirwan, 2024).

5.3. Implications for sandy coasts monitoring and management

The results presented in this study point to the value of integrating field observations across multiple temporal scales and morphodynamic units. The transgressive behavior of the entire coastal profile, characterized by an overall conservation of sediment volume, underscores the importance of considering the full continuum of the nearshore-beach-dune system in coastal management plans.

The city of Ensenada was granted international port status in 1886, followed by the construction of a deep-water pier in the 1920s and the main breakwater in 1956 (Archivo Histórico de Ensenada; https://copladem.ensenada.gob.mx). These large-scale interventions, along with extensive urban development along the coastline, constrain the landward migration of the coastal system in some areas. As is the case in many urbanized coastal regions worldwide, building infrastructure and houses on the backshore limits the capacity for natural transgression. While the study area shows clear evidence of landward migration of dunes, similar responses cannot be expected where infrastructure has been constructed. This highlights the urgent need for integrated coastal zone planning that accounts for the space requirements of dynamic coastal systems under scenarios of rising sea levels.

Vegetation dynamics also play a key role in dune mobility. Although this study did not include an analysis of vegetation cover, existing literature indicates a 65 % decline in vegetation from 1979 to 1998 in the Ensenada dunes, largely due to human activity (Jiménez-Esquivel, 2010). Unregulated pedestrian traffic and vehicle driving contributes to dune degradation (Svenia-Costa, 2011; Delgado-Fernandez et al., 2019). Given the leakage of sediment beyond the dune area measured in this study, and the fact that vegetation can trap wind-blown sand and contribute to dune stabilization, future coastal management plans should incorporate restrictions on human trampling, the restoration of native vegetation, and the designation of conservation zones to protect the sediment budgets. These measures could help counteract severe El Niño winters.

Finally, predominant winds in Ensenada from the northwest (onshore) are relatively weak in comparison with sporadic, strong offshore winds (see Section 2) during the fall and winter. The observed net landward migration of the dunes suggests a significant role for persistent onshore aeolian transport, but future research should explore the relative contributions of wind events of varying intensity, direction, and duration to seasonal and interannual morphological changes. These analyses, along with results presented in this study, could be used to inform numerical modelling to explore the effects of different management scenarios, changes to storminess and projected sea-level rise.

6. Conclusions

This study revealed how El Niño events influence shoreline evolution and sediment balance across the entire shore-beach-dune profile in southern Ensenada, Baja California, Mexico. The 1 km stretch of beach studied, characterized by a mobile dune ridge migrating landward, showed distinct alongshore morphodynamic responses at multiple temporal scales. Multi-decadal shoreline variations (1984–2021) indicate that the powerful 1997–1998 El Niño event forced a retreat of the shoreline to a new average position, marking a stepwise long-term recession that reflects the transgressive behavior of the beach.

Interannual and seasonal analyses of topo-bathymetric surveys (2014–2020) reveal a relatively stable shoreline, oscillating seasonally around a mean position. In contrast, dunes migrated landward at an average rate of approximately 5 m/yr, decoupled from the beach system but maintaining a relatively stable sediment balance. This migration was facilitated by predominantly onshore winds and the absence of vegetation. A one-way connection between the beach and the dune was observed after El Niño events, which formed very high winter-berms. These berms were not eroded by wave action but were gradually reworked by aeolian processes that transported sand to the former dune ridge through the dune toe.

Sediment inputs from the supratidal winter-berms partially compensated for inland dune sand losses; however, an average alongshore sediment leakage of approximately 10 m^3/m occurred over the six-year study period. Despite these losses, the overall sediment budget for the entire shore–beach–dune profile showed a net gain of +40 m^3/m, primarily due to inputs from the subtidal zone. This indicates that the beach can continue to offset sand losses to the dune. Furthermore, the shallow shoreface offshore of Ensenada beach may store remnant sand deposits from past high-energy erosional events, which could be remobilized and transported onshore under favorable conditions, contributing to the beach sediment budget.

This investigation highlights the complexity of transgressive shore-beach-dune systems, which can migrate landward while maintaining their overall volume in response to intense wave events such as El Niño. The beach appears to be forced landward by the transgressive behavior of the dune, which transfers sediment inland and effectively decouples from the original beach-dune system. Looking forward, increased storm activity and sea-level rise are expected to accelerate this landward migration; however, sediment balance may be sustained if offshore inputs continue to supply the system.

Our findings highlight the need to develop monitoring systems that enable multiscale observations of the entire nearshore–beach–dune system, in order to adequately assess its response and adaptation to

environmental changes such as increased storminess and sea-level rise.

CRediT authorship contribution statement

Amaia Ruiz de Alegría-Arzaburu: Writing – review & editing, Writing – original draft, Methodology, Investigation, Funding acquisition, Formal analysis, Data curation, Conceptualization. **Susana Costas:** Writing – review & editing, Writing – original draft, Methodology, Investigation, Conceptualization. **Irene Delgado-Fernández:** Writing – review & editing, Writing – original draft, Methodology, Investigation, Conceptualization.

Declaration of competing interest

The authors declare that they have no known competing financial interests or personal relationships that could have appeared to influence the work reported in this paper.

Acknowledgements

This research was funded by the Mexican CONACYT (now SECIHTI) projects CB-2014-238765 and INFR-2013-205020, and supported by UABC projects 624 ERPLENS (Conv. 17), 636 IMTENS (Conv. 18) and 11720. We acknowledge the support of the UABC Coastal Morphodynamics Research Group (www.mordics.org), particularly the assistance of Ernesto Carsolio, Tadashi Kono and Julio López during fieldwork. We also thank J. Adrián Vidal for his help with some data processing. This work was conducted during Amaia Ruiz de Alegría-Arzaburu's research stays and sabbatical periods in 2021 and 2025 of, in collaboration with the University of Cádiz in Spain. Susana Costas would like to acknowledge the financial support of the Portuguese Foundation for Science and Technology (FCT) through 2021.04286.CEECIND and CEECINSTLA/00018/2022 individual contracts and to CIMA (UID/0350/2020) and ARNET (LA/P/0069/2020).

Data availability

Data will be made available on request.

References

Aagaard, T., Davidson-Arnott, R., Greenwood, B., Nielsen, J., 2004. Sediment supply from shoreface to dunes: linking sediment transport measurements and long-term morphological evolution. Geomorphology 60 (1), 205–224. https://doi.org/10.1016/j.geomorph.2003.08.002.

Barnard, P.L., Hoover, D., Hubbard, D.M., Snyder, A., Ludka, B.C., Allan, J., Kaminsky, G. M., Ruggiero, P., Gallien, T.W., Gabel, I., McCandless, D., Weiner, H.M., Cohn, N., Anderson, D.L., Serafin, L.A., 2017. Extreme oceanographic forcing and coastal response due to the 2015–2016 El Niño. Nat. Commun. 8, 14365. https://doi.org/10.1038/ncomms14365.

Bristow, C.S., Chroston, P.N., Bailey, S.D., 2000. The structure and development of foredunes on a locally prograding coast: insights from ground-penetrating radar surveys, Norfolk, UK. Sedimentology 47, 923–944. https://doi.org/10.1046/j.1365-3091.2000.00330.x.

Burvingt, O., Castelle, B., 2023. Storm response and multi-annual recovery of eight coastal dunes spread along the Atlantic coast of Europe. Geomorphology 435, 108735. https://doi.org/10.1016/j.geomorph.2023.108735.

Carrillo–Rodríguez, O., 2016. Caracterización del campo de dunas "La Lagunita", en la playa Municipal de Ensenada, B.C. Facultad de Ciencias Marinas, Universidad Autónoma de Baja California, tesis de licenciatura.

Carriquiry–Beltrán, J.D., 1985. Análisis de la distribución de materiales pesados presentes en los sedimentos clásicos de la Bahía de Todos Santos, B.C.: Ensenada, Baja California, Facultad de Ciencias Marinas, Universidad Autónoma de Baja California, Ensenada, B.C., México. MSc Thesis..

Castelle, B., Bujan, S., Ferreira, S., Dodet, G., 2017. Foredune morphological changes and beach recovery from the extreme 2013/2014 winter at a high-energy sandy coast. Mar. Geol. 385, 41–55. https://doi.org/10.1016/j.margeo.2016.12.006.

Costas, S., 2022. Evolutionary trajectories of coastal sand barriers along the west Portuguese coast during the Holocene. J. Mar. Sci. Eng. 10 (12), 1894. https://doi.org/10.3390/jmse10121894.

Costas, S., Ferreira, O., Plomaritis, T.A.T.A., Leorri, E., Ferreira, Ó., Plomaritis, T.A.T.A., Leorri, E., 2016. Coastal barrier stratigraphy for Holocene high-resolution sea-level reconstruction. Sci. Rep. 6, 38726. https://doi.org/10.1038/srep38726.

Costas, S., Gallego-Fernández, J.B., de Sousa, L.B., Kombiadou, K., 2023. Ecogeomorphic response of a coastal dune in southern Portugal regulated by extrinsic factors. Catena 221, 106796. https://doi.org/10.1016/j.catena.2022.106796.

Cowell, P.J., Roy, P.S., Jones, R.A., 1995. Simulation of large-scale coastal change using a morphological behaviour model. Mar. Geol. 126, 45–61. https://doi.org/10.1016/0025-3227(95)00065-7.

Curray, J.R., 1964. Transgressions and regressions. In: Miller, R.L. (Ed.), Papers in Marine Geology. Macmillan, New York, pp. 175–203.

DaSilva, M.D., Hesp, P.A., Bruce, D., Downes, J., da Silva, G.M., 2024. Coastal transgressive dunefield evolution as a response to multi-decadal shoreline erosion. Geomorphology 455, 109165. https://doi.org/10.1016/j.geomorph.2024.109165.

Davidson-Arnott, R.G.D., 2005. A conceptual model of the effects of sea level rise on sandy coasts. J. Coastal Res. 21 (6), 1166–1172. https://doi.org/10.2112/03-0051.1.

Davidson-Arnott, R.G.D., Bauer, B.O., 2021. Controls on the geomorphic response of beach-dune systems to water level rise. J. Great Lakes Res. 47 (6), 1594–1612. https://doi.org/10.1016/j.jglr.2021.05.006.

Davidson-Arnott, R., Hesp, P., Ollerhead, J., Walker, I., Bauer, B., Delgado-Fernandez, I., Smyth, T., 2018. Sediment budget controls on foredune height: comparing simulation model results with field data. Earth Surf. Process. Landf. https://doi.org/10.1002/esp.4354.

Davidson-Arnott, R., Ollerhead, J., George, E., Houser, C., Bauer, B., Hesp, P., Walker, I., Delagado-Fernandez, I., van Proosdij, D., 2024. Assessing the impact of hurricane Fiona on the coast of PEI National Park and implications for the effectiveness of beach-dune management policies. J. Coast. Conserv. 28 (3), 52. https://doi.org/10.1007/s11852-024-01050-5.

Dean, R.G., 1973. Heuristic models of sand transport in the surf zone. In: Proc. Conf. Eng. Dynamics Surf Zone, Sydney, pp. 208–214. https://doi.org/10.3316/informit.971703171672500.

Delgado-Fernández, I., Davidson-Arnott, R.D.A., 2011. Meso-scale aeolian sediment input to coastal dunes: the nature of aeolian transport events. Geomorphology 126 (1), 217–232. https://doi.org/10.1016/j.geomorph.2010.11.005.

Delgado-Fernandez, I., O'Keeffe, N., Davidson-Arnott, R.G., 2019. Natural and human controls on dune vegetation cover and disturbance. Sci. Total Environ. 672, 643–656. https://doi.org/10.1016/j.scitotenv.2019.03.494.

Fischer, A.G., 1961. Stratigraphic record of transgressing seas in light of sedimentation on Atlantic coast of New Jersey. AAPG Bull. 45, 1656–1666. https://doi.org/10.1306/BC743717-16BE-11D7-8645000102C1865D.

Goldsmith, V., 1973. Internal geometry and origin of vegetated coastal sand dunes. J. Sediment. Petrol. 43, 1128–1142. https://doi.org/10.1306/74D72923-2B21-11D7-8648000102C1865D.

González-Yajimovich, O., 1981. Transporte eólico en una porción de playa de la Bahía de Todos Santos, Baja California. Escuela Superior de Ciencias Marinas. UABC (32 pp., BSc Thesis).

Harley, M., Masselink, G., Ruiz de Alegría-Arzaburu, A., Scott, T., Valiente, N., 2022. Single extreme storm sequence can offset decades of shoreline retreat projected to result from sea-level rise. Nat. Commun. Earth Environ. 3, 112. https://doi.org/10.1038/s43247-022-00437-2.

Hein, C.J., Kirwan, M.L., 2024. Marine transgression in modern times. Annu. Rev. Mar. Sci. 16, 55–79. https://doi.org/10.1146/annurev-marine-022123-103802.

Herrero, X., Costas, S., Kombiadou, K., 2020. Coastal ridge constructive processes at a multi-decadal scale in Barreta Island (southern Portugal). Earth Surf. Process. Landf. 45, 411–423. https://doi.org/10.1002/esp.4742.

Hersbach, H., et al., 2020. The ERA5 global reanalysis. Q. J. R. Meteorol. Soc. 146, 1999–2049. https://doi.org/10.1002/qj.3803.

Hesp, P.A., 1988. Morphology, dynamics and internal stratification of some established foredunes in southeast Australia. Sediment. Geol. 55, 17–41. https://doi.org/10.1016/0037-0738(88)90088-7.

Hesp, P., 2002. Foredunes and blowouts: initiation, geomorphology and dynamics. Geomorphology 48 (1–3), 245–268. https://doi.org/10.1016/s0169-555x(02)00184-8.

Hesp, P., 2013. Conceptual models of the evolution of transgressive dune field systems. Geomorphology 199, 138–149. https://doi.org/10.1016/j.geomorph.2013.05.014.

Hesp, P.A., DaSilva, M., Miot da Silva, G., Bruce, D., Keane, R., 2022. Review and direct evidence of transgressive aeolian sand sheet and dunefield initiation. Earth Surf. Process. Landf. 47, 2660–2675. https://doi.org/10.1002/esp.5400.

Houser, C., 2018. Barrier response to sea level rise and storms. Earth Surf. Process. Landf. 43 (11), 2481–2483. https://doi.org/10.1002/esp.4396.

Houser, C., Hapke, C., Hamilton, S., 2008. Controls on coastal dune morphology, shoreline erosion and barrier island response to extreme storms. Geomorphology 100, 223–240. https://doi.org/10.1016/j.geomorph.2007.12.007.

Jiménez-Esquivel, V.M., 2010. Cambios en la vegetación de dunas costeras de la playa municipal de Ensenada entre los años 1979,1980,1993 y 1998. Trabajo terminal de especialidad en gestión ambiental. Faculta de Ciencias Marinas. Universidad Autónoma de Baja California, Ensenada, Baja California, México (43 pp.).

Kombiadou, K., Matias, A., Ferreira, O., Carrasco, A.R., Costas, S., Plomaritis, T., 2019. Impacts of human interventions on the evolution of the Ria Formosa barrier island system (S. Portugal). Geomorphology 343, 129–144. https://doi.org/10.1016/j.geomorph.2019.07.006.

Lancaster, N., Helm, P., 2000. A test of a climatic index of dune mobility using measurements from the southwestern United States. Earth Surf. Process. Landf. 25 (2), 197–207. https://doi.org/10.1002/(SICI)1096-9837(200002)25:2<197:AID-ESP82>3.0.CO;2-H.

Laporte-Fauret, Q., Castelle, B., Marieu, V., Nicolae-Lerma, A., Rosebery, D., 2022. Foredune blowout formation and subsequent evolution along a chronically eroding

high-energy coast. Geomorphology 414, 108398. https://doi.org/10.1016/j.geomorph.2022.108398.
Leatherman, S.P., 1983. Barrier dynamics and landward migration with Holocene sea-level rise. Nature 301 (5899), 415–417. https://doi.org/10.1038/301415a0.
Lizarraga-Arciniega, R., Chee-Barragán, A., Gil-Silva, E., Mendoza-Ponce, T., Martínez-Díaz de León, A., 2003. Effect of El Niño on the subaerial beach Playas de Rosarito, B.C., Mexico. Geofis. Int. 42 (3), 419–428. https://doi.org/10.22201/igeof.00167169p.2003.42.3.924.
Lorenzo-Trueba, J., Ashton, A.D., 2014. Rollover, drowning, and discontinuous retreat: distinct modes of barrier response to sea-level rise arising from a simple morphodynamic model. J. Geophys. Res. Earth. https://doi.org/10.1002/2013JF002941.
Masselink, G., van Heteren, S., 2014. Response of wave-dominated and mixed-energy barriers to storms. Mar. Geol. 352, 321–347. https://doi.org/10.1016/j.margeo.2013.11.004.
Masselink, G., Brooks, S., Poate, T., Stokes, C., Scott, T., 2022. Coastal dune dynamics in embayed settings with sea-level rise – examples from the exposed and macrotidal north coast of SW England. Mar. Geol. 450, 106853. https://doi.org/10.1016/j.margeo.2022.106853.
Miot da Silva, G., Hesp, P., Keim, B., Martinho, C.T., Ferligoj, Y., 2013. Changes in dunefield geomorphology and vegetation cover as a response to local and regional climate variations. In: Conley, D.C., Masselink, G., Russell, P.E., O'Hare, T.J. (Eds.), Proceedings 12th International Coastal Symposium (Plymouth, England), Journal of Coastal Research, pp. 1307–1312. https://doi.org/10.2112/SI65-221.1 (SI65)0749-0208.
Moore, L.J., Durán Vinent, O., Ruggiero, P., 2016. Vegetation control allows autocyclic formation of multiple dunes on prograding coasts. Geology 44 (7), 559–562. https://doi.org/10.1130/G37778.1.
Nienhuis, J.H., Lorenzo-Trueba, J., 2019. Can barrier Islands survive sea-level rise? Quantifying the relative role of tidal inlets and overwash deposition. Geophys. Res. Lett. https://doi.org/10.1029/2019GL085524.
Oderiz, I., Silva, R., Mortlock, T.R., Mori, N., 2020. ENSO impacts on global wave climate and potential coastal hazards. J. Geophys. Res. Oceans. https://doi.org/10.1029/2020JC016464.
Ollerhead, J., Davidson-Arnott, R., Walker, I.J., Mathew, S., 2013. Annual to decadal morphodynamics of the foredune system at Greenwich Dunes, Prince Edward Island, Canada. Earth Surf. Process. Landf. 38 (3), 284–298. https://doi.org/10.1002/esp.3327.
Ollerhead, J., Davidson-Arnott, R., Bauer, B., 2022. The importance of coastal foredunes as a nature-based solution for shoreline protection: what Hurricane Fiona tells us, Canadian Meteorological and Oceanographic Bulletin. https://bulletin.cmos.ca/the-importance-of-coastal-foredunes-as-a-nature-based-solution-for-shoreline-protection-what-hurricane-fiona-tellsus.
Provoost, S., Jones, M.L.M., Edmondson, S.E., 2011. Changes in landscape and vegetation of coastal dunes in northwest Europe: a review. J. Coast. Conserv. https://doi.org/10.1007/s11852-009-0068-5.
Psuty, N.P., 1988. Sediment budget and dune/beach interaction. J. Coast. Res. (SI 3), 1–4. https://www.jstor.org/stable/40928719.
Psuty, N.P., 2004. The coastal foredune: a morphological basis for regional coastal dune development. In: Martinez, M.L., Psuty, N.P. (Eds.), Coastal Dunes. Ecology and Conservation. Springer, Berlin, pp. 11–27.
Rodríguez, A.B., Theuerkauf, E.J., Ridge, J.T., VanDusen, B.M., Fegley, S.R., 2020. Long-term washover fan accretion on a transgressive barrier island challenges the assumption that paleotempestites represent individual tropical cyclones. Sci. Rep. 10, 19755. https://doi.org/10.1038/s41598-020-76521-4.
Roy, P.S., Thom, B.G., Wright, L.D., 1980. Holocene sequences on an embayed high-energy coast: an evolutionary model. Sediment. Geol. 26, 1–19. https://doi.org/10.1016/0037-0738(80)90003-2.
Ruggiero, P., Hacker, S., Seabloom, E., Zarnetske, P., 2018. The role of vegetation in determining dune morphology, exposure to sea-level rise, and storm-induced coastal hazards: a U.S. Pacific Northwest perspective. In: Moore, L., Murray, A. (Eds.), Barrier Dynamics and Response to Changing Climate. Springer, Cham. https://doi.org/10.1007/978-3-319-68086-6_11.
Ruiz de Alegría-Arzaburu, A., Vidal-Ruiz, J.A., 2018. Beach recovery capabilities after El Niño 2015–2016 at Ensenada Beach, Northern Baja California. Ocean Dyn. https://doi.org/10.1007/s10236-018-1164-6.
Ruiz de Alegría-Arzaburu, A., Vidal-Ruiz, J.A., García-Nava, H., Romero-Arteaga, A., 2017. Seasonal morphodynamics of the subaerial and subtidal sections of an intermediate and mesotidal beach. Geomorphology 295, 383–392. https://doi.org/10.1016/j.geomorph.2017.07.021.
Ruiz de Alegría-Arzaburu, A., Gasalla-López, B., Benavente, J., 2022. Morphological response of an embayed beach to swell-driven storminess cycles over an 8-year period. Geomorphology 403, 108164. https://doi.org/10.1016/j.geomorph.2022.108164.
Sallenger Jr., A.H., Krabill, W., Brock, J., Swift, R., Manizade, S., Stockdon, H., 2002. Sea-cliff erosion as a function of beach changes and extreme wave runup during the 1997–1998 El Niño. Mar. Geol. 187 (3–4), 279–297. https://doi.org/10.1016/S0025-3227(02)00316-X.
Sherman, D.J., Bauer, B.O., 1993. Dynamics of beach-dune systems. Prog. Phys. Geogr. Earth Environ. 17 (4), 413–447. https://doi.org/10.1177/030913339301700402.
Short, A.D., Hesp, P.A., 1982. Wave, beach and dune interactions in southeastern Australia. Mar. Geol. 48 (3–4), 259–284. https://doi.org/10.1016/0025-3227(82)90100-1.
Smith, A., Houser, C., Lehner, J., George, E., Lunardi, B., 2020. Crowd-sourced identification of the beach-dune interface. Geomorphology 367, 107321. https://doi.org/10.1016/j.geomorph.2020.107321.
Storlazzi, C.D., Willis, C.M., Griggs, G.B., 2000. Comparative impacts of 1982–83 and 1997–98 El Niño winter son the Central California coast. J. Coast. Res. 16 (4), 1022–1036.
Svenia-Costa, S., 2011. Evaluación de la vulnerabilidad de las dunas costeras de la Bahía de Todos Santos, B.C. Trabajo terminal de especialidad en gestión ambiental. Faculta de Ciencias Marinas. Universidad Autónoma de Baja California, Ensenada, Baja California, México (50 pp.).
Talavera, L., Costas, S., Ferreira, O., 2024. Control son blowout evolution in southern Portugal: a 49-year analysis. Sci. Total Environ. 955, 176769. https://doi.org/10.1016/j.scitotenv.2024.176769.
Vidal-Ruiz, J.A., Ruiz de Alegría-Arzaburu, A., 2019. Variability of sandbar morphometrics over three seasonal cycles on a single-barred beach. Geomorphology 333, 61–72. https://doi.org/10.1016/j.geomorph.2019.02.034.
Vidal-Ruiz, J.A., Ruiz de Alegría-Arzaburu, A., 2020. Modes of onshore sandbar migration at a single-barred and swell-dominated beach. Mar. Geol. 426, 106222. https://doi.org/10.1016/j.margeo.2020.106222.I.
Vos, K., Harley, M.D., Splinter, K.D., Simmons, J.A., Turner, I.L., 2019a. Sub-annual to multi-decadal shoreline variability from publicly available satellite imagery. Coast. Eng. 150, 160–174. https://doi.org/10.1016/j.coastaleng.2019.04.004.
Vos, K., Splinter, K.D., Harley, M.D., Simmons, J.A., Turner, I.L., 2019b. Coastsat: a Google earth engine-enabled Python toolkit to extract shorelines from publicly available satellite imagery. Environ. Model. Softw. 122, 104528. https://doi.org/10.1016/j.envsoft.2019.104528.
Vos, K., Harley, M.D., Turner, I.L., Splinter, K.D., 2023. Pacific shoreline erosion and accretion patterns controlled by El Niño/Southern Oscillation. Nat. Geosci. 16, 140–146.
Walker, I.J., Davidson-Arnott, R.G.D., Bauer, B.O., Hesp, P.A., Delgado-Fernandez, I., Ollerhead, J., Smyth, T.A.G., 2017. Scale-dependent perspectives on the geomorphology and evolution of beach-dune systems. Earth Sci. Rev. 171, 220–253. https://doi.org/10.1016/j.earscirev.2017.04.011.